Supporting information

Unravelling the morphological dependency of the $LiNi_{0.6}Mn_{0.2}Co_{0.2}O_2$ layered oxide reactivity in Li-ion batteries

Adrien Soloy[1], Delphine Flahaut[2,5], Jean-Bernard Ledeuil[2,5], Joachim Allouche[2,5], Dominique Foix[2,5], Germain Salvato Vallverdu[2,5], Emmanuelle Suard[3], Erwan Dumont[4], Lucille Gal[4], François Weill[1,5,6,] and Laurence Croguennec[1,5,6,*]*

[1] Univ. Bordeaux, CNRS, Bordeaux INP, ICMCB UMR 5026, F-33600 Pessac, France

[2] Université de Pau et des Pays de l'Adour, E2S UPPA, CNRS, IPREM UMR 5254, 64000 Pau, France

[3] Institut Laue-Langevin, 71 avenue des Martyrs, 38042 Grenoble, France

[4] SAFT, Direction de la Recherche, 33074 Bordeaux, France

[5] RS2E, Réseau Français sur le Stockage Electrochimique de l'Energie, FR CNRS 3459, F-80039 Amiens Cedex 1, France

[6] ALISTORE-ERI European Research Institute, FR CNRS 3104, F-80039 Amiens Cedex 1, France

* Laurence.Croguennec@icmcb.cnrs.fr; Francois.weill@icmcb.cnrs.fr (corresponding authors)

Table S1. Chemical analyses of the synthesized samples performed by ICP-OES.

	ICP-OES			
	Ni/∑xTM	**Mn/∑xTM**	**Co/∑xTM**	**Li/∑xTM**
870-5-air	0.62(6)	0.19(2)	0.19(1)	1.0(1)
17-PL	0.6(1)	0.20(2)	0.20(2)	1.1(1)
86-PL	0.62(5)	0.19(2)	0.19(1)	1.00(8)

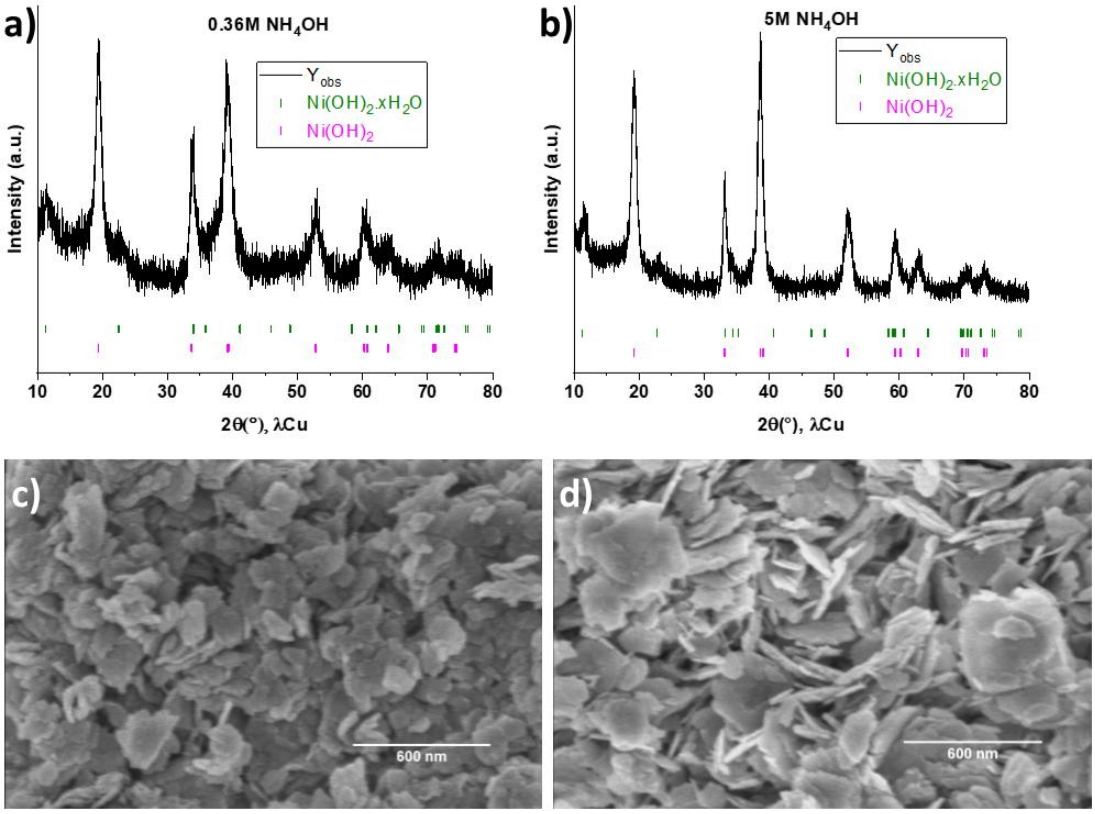

Figure S1. XRD patterns (a,b) and SEM pictures (c,d) of the mixed TM hydroxide precursors synthesized by coprecipitation with a low-concentrated (0.36M) NH_4OH solution (a,c) to obtain the conventional NMC622 layered oxide and a highly concentrated (5M) NH_4OH solution (b) to obtain platelet-like NMC622 particles.

When the 0.36M NH_4OH solution is used during the coprecipitation, platelets of around 30 nm thick and 170 nm long are obtained while when the 5M NH_4OH solution is used, platelets of around 15 nm thick and 260 nm long are obtained. This shows that increasing the concentration of the NH_4OH solution during the coprecipitation helps forming particles with a more pronounced platelet shape, with a smaller thickness and a larger length.

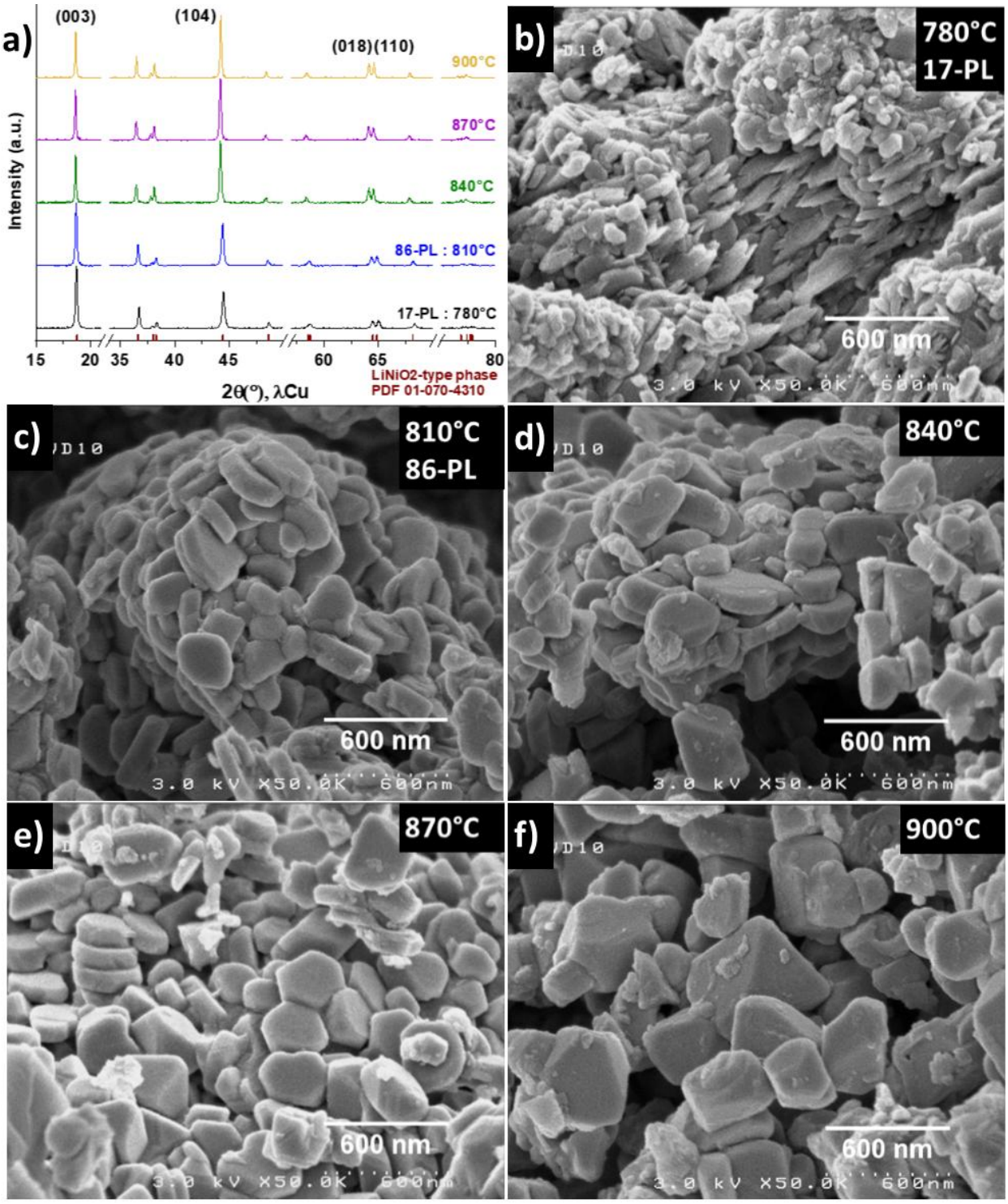

Figure S2. XRD patterns (a) and morphologies (b-f) of the samples synthesized from the transition metal hydroxide obtained by coprecipitation using a highly concentrated 5 mol/L NH4OH aqueous solution. Lithiation to obtain the lithiated layered oxides was performed at 780°C (17-PL sample), 810°C (86-PL sample), 840°C, 870°C or 900°C using Li_2CO_3 as Li precursor. The XRD patterns were obtained after 35 min analyses.

Figure S2 summarizes a preliminary study performed to identify the best synthesis conditions to obtain layered oxides with platelet-like morphologies. **Figure S2a** shows that for the two lowest temperatures, 780°C and 810°C, the intensity of the (003) reflection is obviously higher than that of the (104) diffraction line, whereas when higher temperatures are used the contrary is observed. This observation shows that only the samples obtained at 780°C and 810°C have a structure close to the ideal 2D layered structure.[9,27–29] **Figure S2b-f** shows the morphologies obtained for the five samples synthesized between 780°C and 900°C. Platelet-shaped particles are obtained between 780°C and 840°C with a clear increase of their thickness with increasing temperature. However, it is observed that the platelet morphology tends to disappear at temperatures higher than 870°C in favour of a more prismatic morphology. As they have the structure that is the closest to the ideal 2D one and platelet-shaped particles with different thicknesses, the samples obtained at 780°C and 810°C were selected for further characterizations. They are named respectively 17-PL and 86-PL.

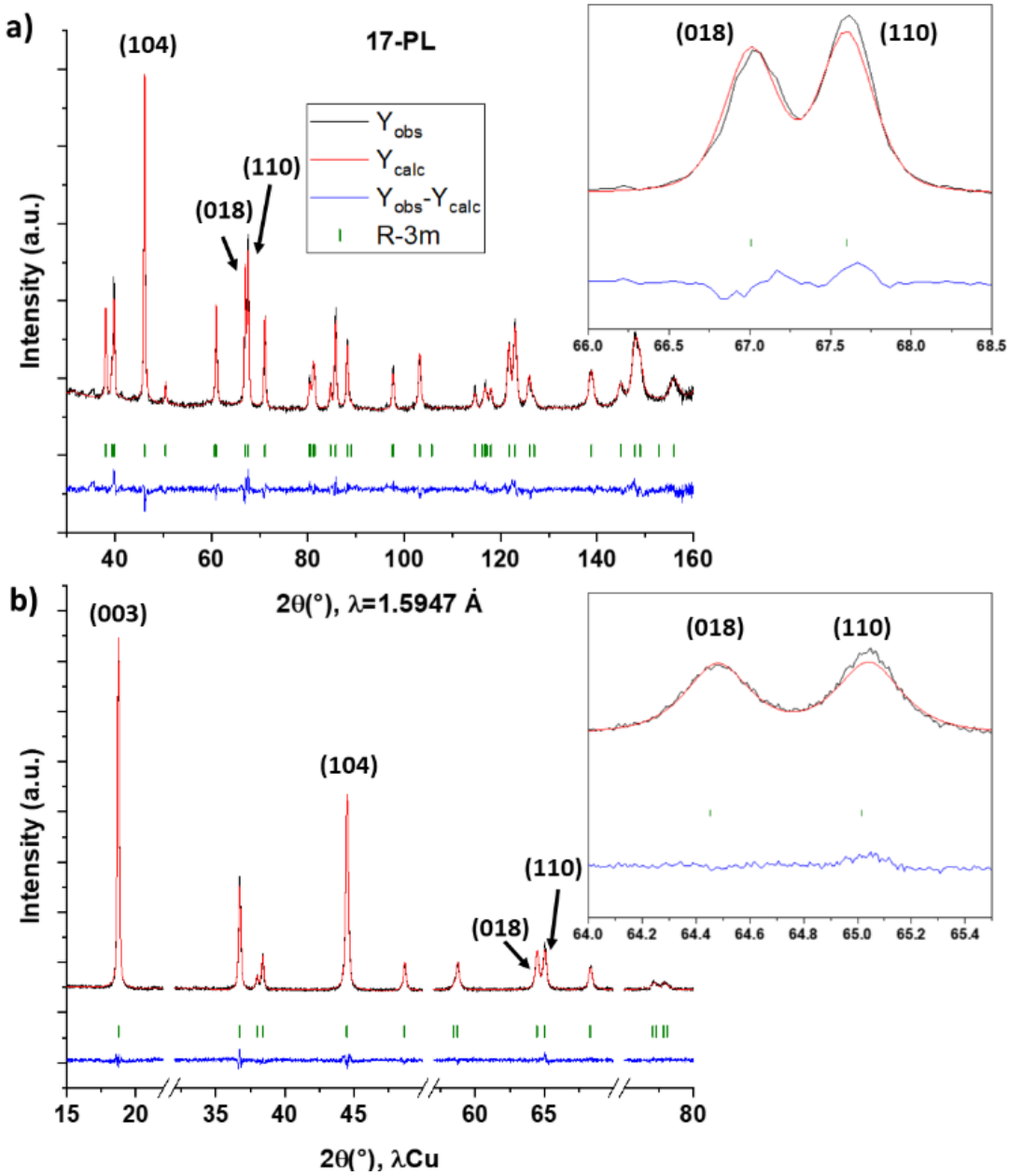

Figure S3. Refinements of the neutron (a) and X-ray (b) diffraction patterns recorded for the 17-PL sample. Axis breaks were used in order to highlight better the quality of the refinements, as shown also by the enlargements of the (018)/(110) diffraction lines given on the right of the figure.

Table S2. Structural parameters determined for the 17-PL sample by the Rietveld refinement of its Neutron (upper line) and X-ray diffraction (lower line, in italics) patterns. On the contrary to neutron diffraction, it is not possible to distinguish Ni, Mn and Co by X-ray diffraction.

17-PL sample Space group: R-3m, Z=3 a =2.86658(9) Å = b; c = 14.208(1) Å; c/a = 4.9564(5) Neutrons: R_{wp} = 3.96%; R_p = 3.13%; R_{bragg} = 6.99%; λ = 1.5947(1) Å XRD : R_{wp} = 3.65%; R_p = 2.89%; R_{bragg} = 4.65%						
Atom	**Wyckoff position**	**x/a**	**y/b**	**z/c**	**Biso**	**Occ.**
Li	3b	0	0	½	1.1(4) 1	0.968(3) 0.973(3)
Ni	3b	0	0	½	1.1(4) 1	0.032(3) 0.027(3)
Ni	3a	0	0	0	1.2(1) 0.08(7)	0.584(3) 1
Mn	3a	0	0	0	1.2(1) /	0.208(0) /
Co	3a	0	0	0	1.2(1) /	0.208(0) /
O	6c	0	0	0.2583(3) 0.2587(3)	1.27(8) 0.0(1)	1 1

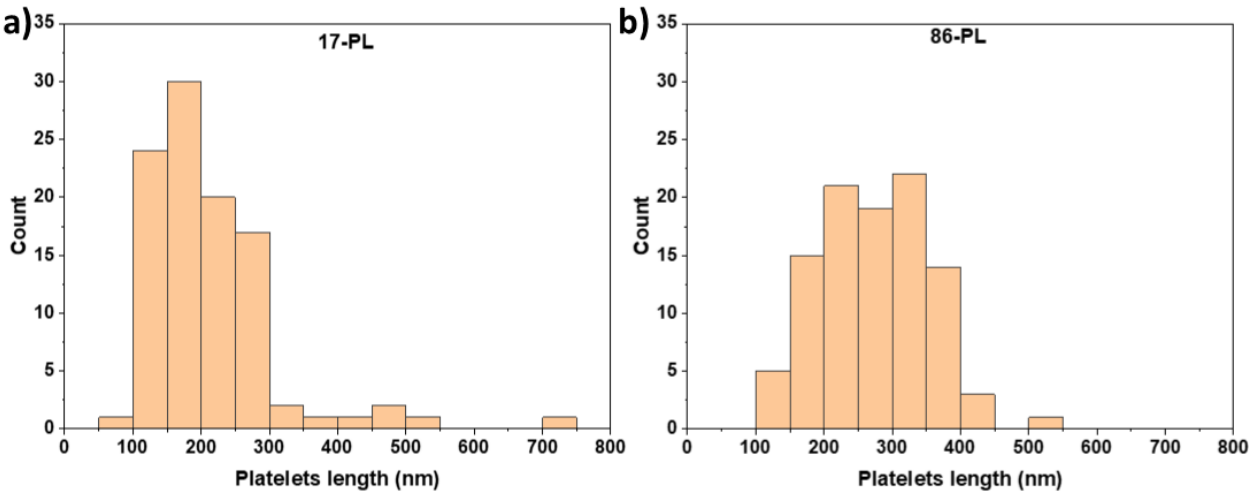

Figure S4. Size distributions obtained from the measurements of the platelet lengths of the 17-PL sample (a) and the 86-PL sample (b) on the SEM pictures.

Table S3. XPS quantitative analyses of the 870-5-air sample (280 nm in diameter particles).

Peak	Assignment	BE (eV)	At. %
C 1s	C-C/C-H	285.0	14.9
	C-O	286.5	1.5
	$C=O/CO_2$	288.6	1.3
	CO3	290.1	11.1
Li 1s	NMC	54.4	3.0
	Li_2CO_3	55.5	23.0
O 1s	NMC	529.7	3.2
	CO_3	531.9	37.0
	C-O	533.6	2.5
Ni 3p	Ni	67.2-74.0	1.6
Co 3p	Co	61.4	0.4
Mn 3p	Mn	49.9-51.9	0.7

Table S4. Transition metal ratios obtained from Ni, Mn and Co atomic percentages extracted from the global quantitative analyses performed from XPS spectra of the three materials.

	Atomic percentages				
	Ni3p	**Co3p**	**Mn3p**	**ΣTM**	**Ni:Mn:Co**
870-5-air	1.6	0.4	0.7	2.7	0.6:0.1:0.3
17-PL	4.3	1.1	1.5	6.8	0.6:0.2:0.2
86-PL	4.2	0.9	1.7	6.8	0.6:0.1:0.3

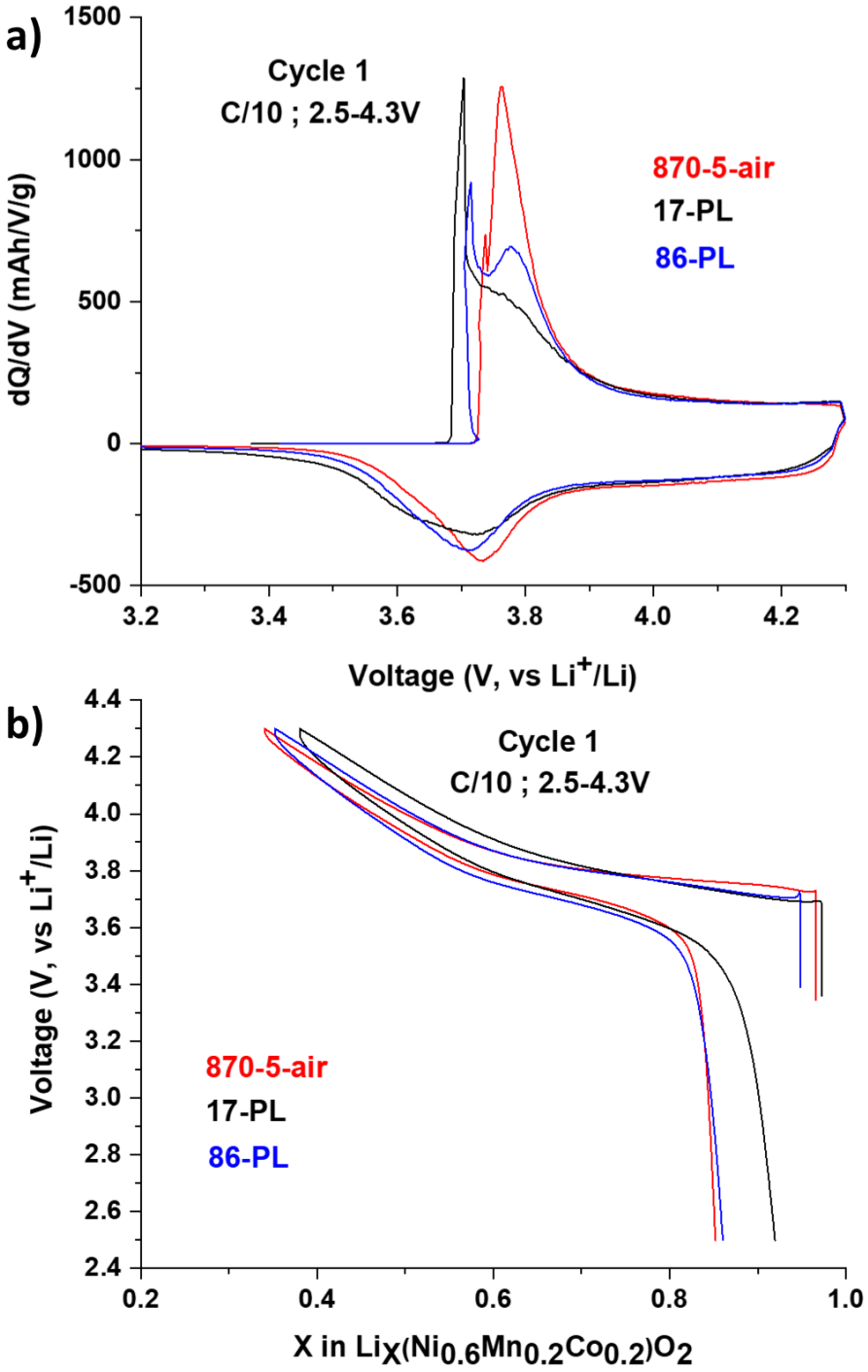

Figure S5. dQ/dV curves (a) and V=f(xLi) cycling curves (b) obtained at 1st cycle at C/10 in the 2.5-4.3 V potential window for the conventional particles (870-5-air), the 17 nm platelets (17-PL) and the 86 nm platelets (86-PL).

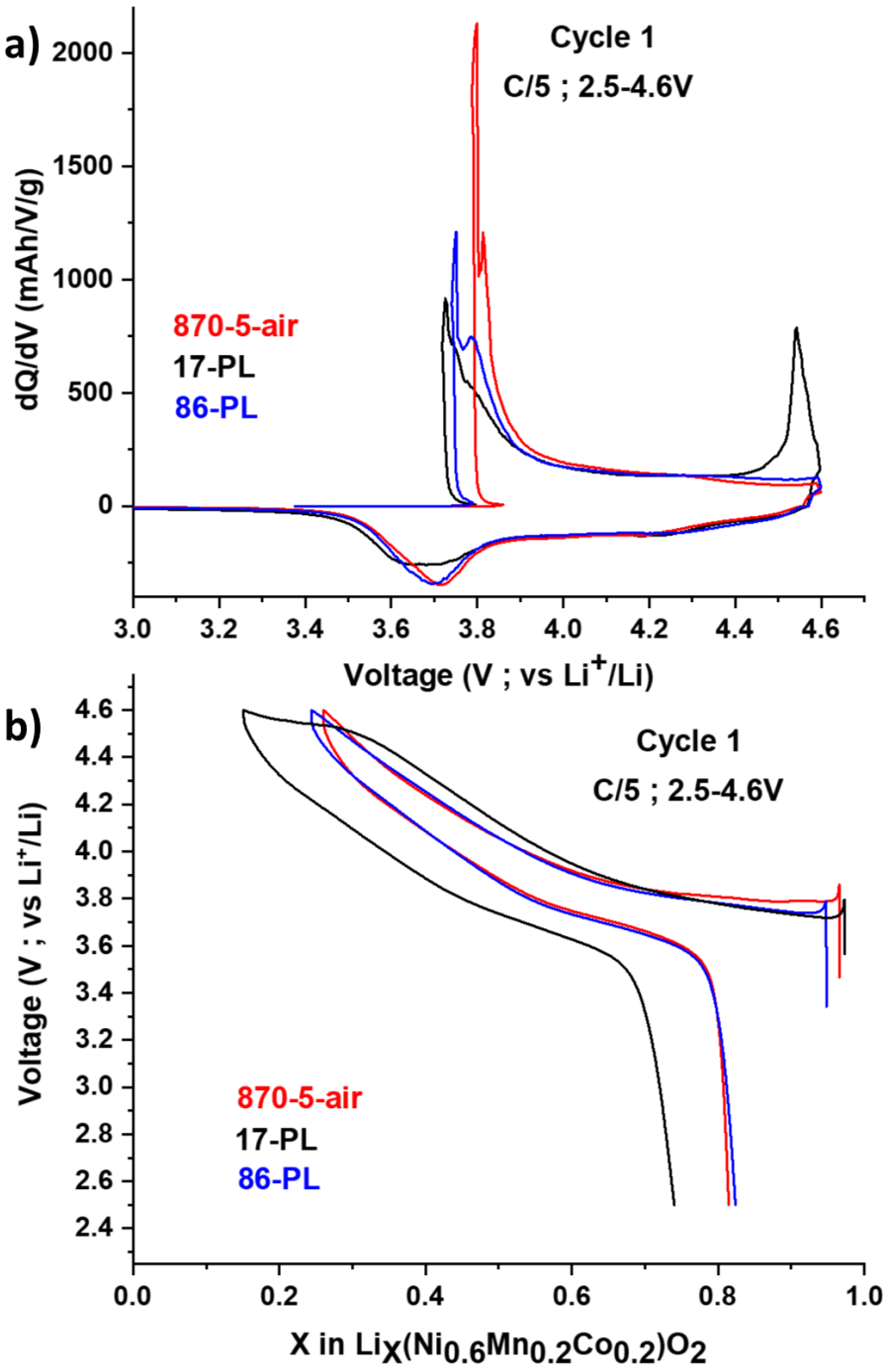

Figure S6. dQ/dV curves (a) and V=f(xLi) cycling curves (b) obtained at 1st cycle at C/5 in the 2.5-4.6 V potential window for the conventional particles (870-5-air), the 17 nm platelets (17-PL) and the 86 nm platelets (86-PL).

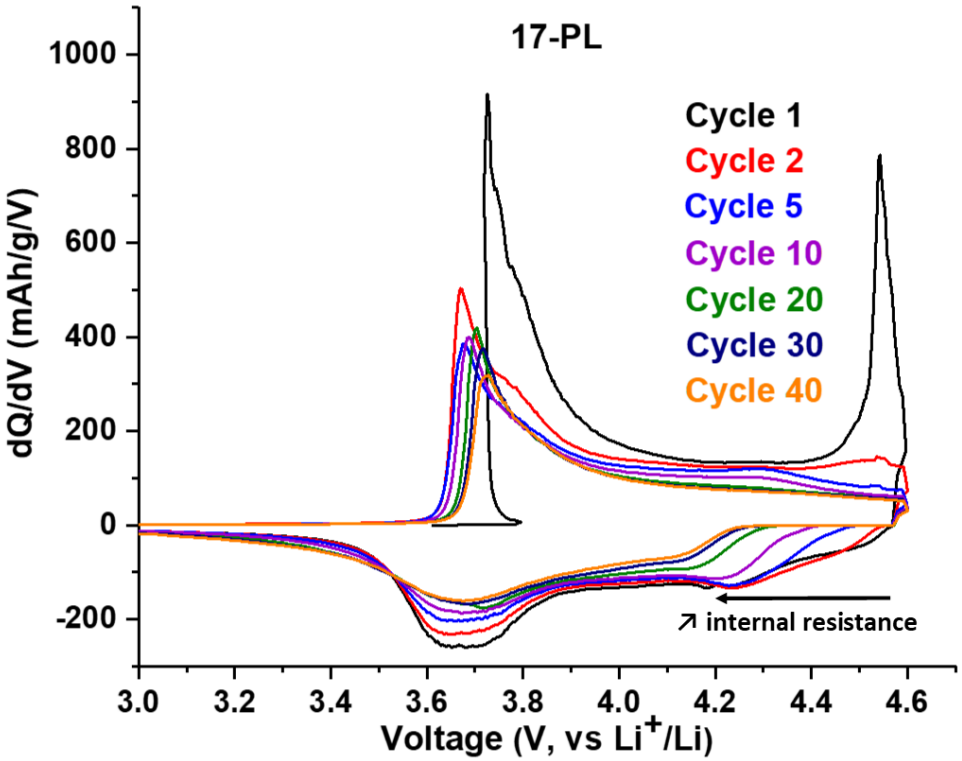

Figure S7. dQ/dV derivative curves corresponding to the cycles 1, 2, 5, 10, 20, 30 and 40 for the 17-PL material (made of 17 nm thick platelets) when cycled at C/5 in the 2.5-4.6 V potential range.

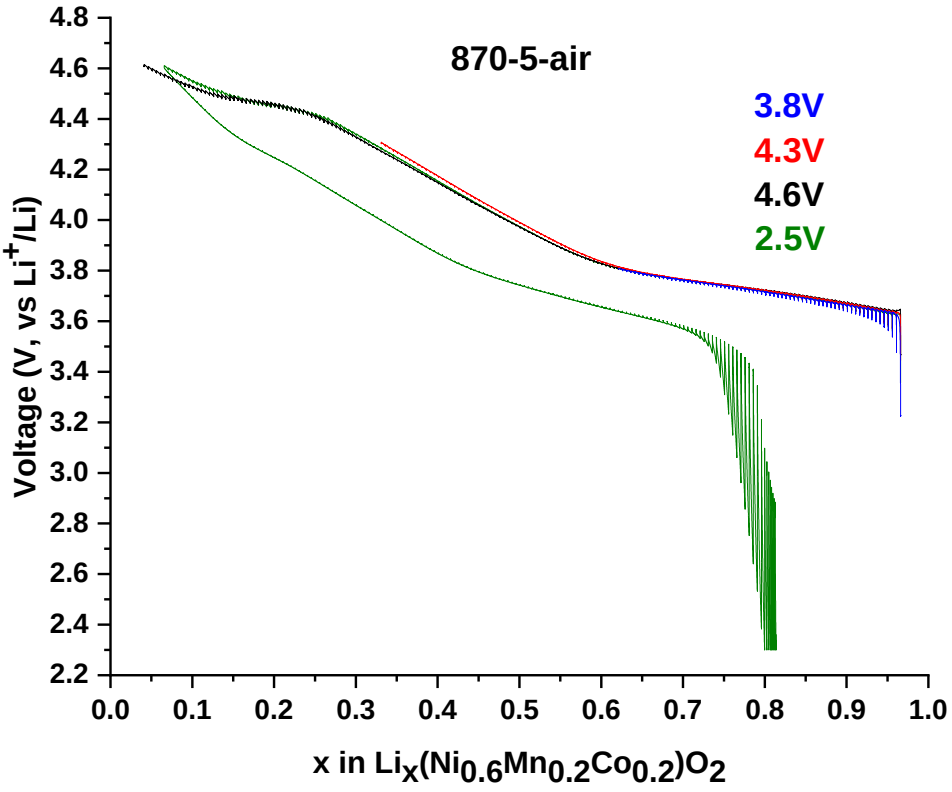

Figure S8. Cycling curves obtained for the different coin cells cycled in GITT conditions for the conventional particles (870-5-air sample) and stopped at 3.8 V, 4.3 V, 4.6 V and 2.5 V.

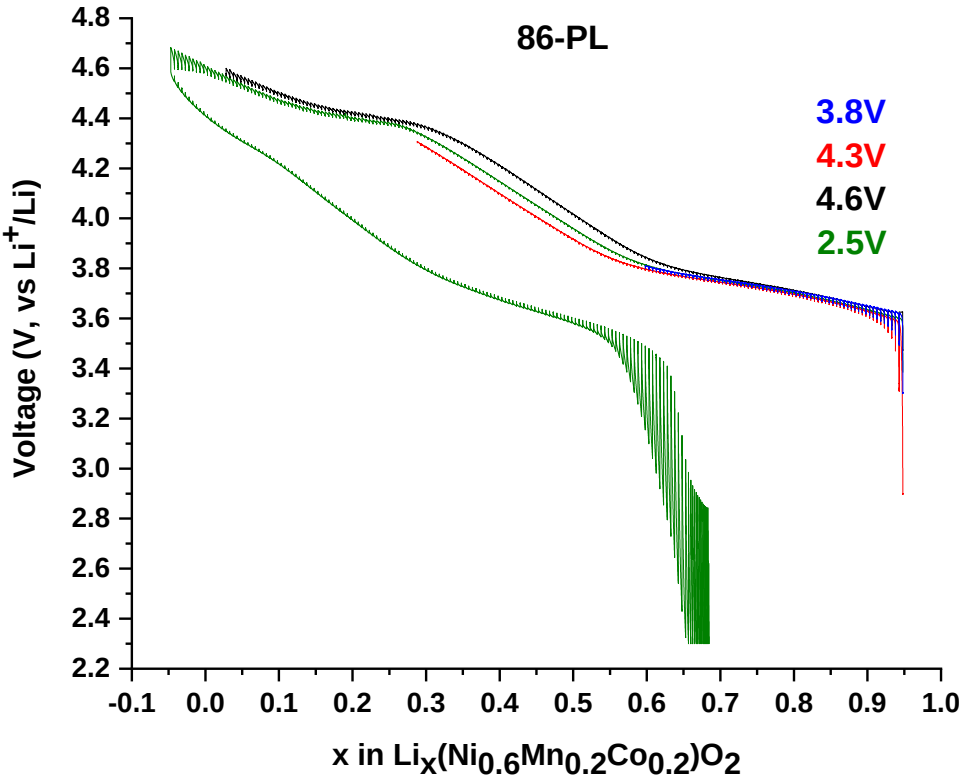

Figure S9. Cycling curves obtained for the different coin cells cycled in GITT conditions for the 86 nm platelets (86-PL sample) and stopped at 3.8V, 4.3V, 4.6V and 2.5V.

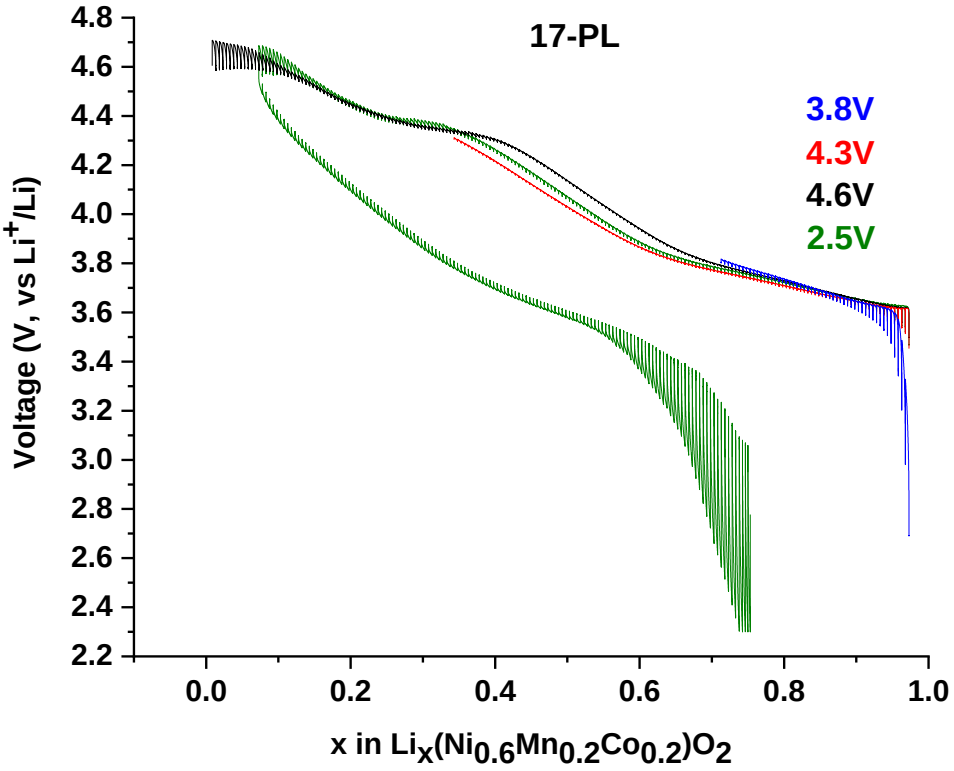

Figure S10. Cycling curves obtained for the different coin cells cycled in GITT conditions for the 17 nm platelets (17-PL sample) and stopped at 3.8V, 4.3V, 4.6V and 2.5V.

Table S5. XPS quantitative surface analysis of the 870-5-air sample (280 nm in diameter particles) after being recovered at 4.3V vs Li^+/Li at the end of the 1st charge.

Peak	Assignment	BE (eV)	At. %
C1s	C-C/C-H	285.1	4.5
	C-O	286.4	3.0
	C=O	287.6	1.6
	CO_2	289.2	1.5
	CO_3	290.1	1.6
	CB	284.4	19.7
	CH_2 PVDF	286.5	4.2
	CF_2 PVDF	291.0	4.2
Li1s	NMC	54.3	3.3
	Li_2CO_3	55.3	3.8
	$LiF/Li_xPF_yO_z$	56.3	13.2
O1s	NMC	530.0	0.9
	CO_3, CO_2	531.7	5.5
	CO_2, O-C	532.8	5.7
	O-P	534.3	2.1
Ni3p	Ni	68.8	0.5
Co3p	Co	61.0	0.1
Mn3p	Mn	50.0	0.3
P2p	$Li_xPF_yO_z$	135.1	1.6
F1s	LiF	685.2	9.2
	CF_2 PVDF	688.3	10.0
	$Li_xPF_yO_z$	686.5	2.9
	CF_3 PVDF	690.0	0.7

Table S6. Comparison of the contributions in atomic percentages of carbon black (CB), PVDF, active material (AM), $LiF/Li_xPF_yO_z$ species and carbonaceous species extracted from the global quantitative surface analyses made from XPS spectra of the 870-5-air electrodes recovered at different states of charge and discharge during the 1st cycle. They are compared to the contributions obtained for the corresponding pristine and OCV electrodes.

870-5-air	Pristine electrode	OCV	3.8V	4.3V	4.6V	2.5V
At.% Carbon black (CB)	23.6	20.9	26.7	19.7	17.5	7.7
At.% PVDF	14.4	24.0	17.3	19.2	21.2	16.8
At.% Active material (AM)	9.0	2.7	4.3	5.0	6.5	2.7
At.% $LiF/Li_xPF_yO_z$	2.2	26.9	15.2	28.9	23.4	34.7
At.% Carbonaceous species	50.0	25.3	36.7	27.2	30.8	38.2

Table S7. Comparison of the contributions in atomic percentages of carbon black (CB), PVDF, active material (AM), LiF/$Li_xPF_yO_z$ species and carbonaceous species extracted from the global quantitative surface analyses performed from XPS spectra of electrodes made of the 86-PL sample and recovered at different states of charge and discharge during the 1st cycle. They are compared to the contributions obtained for the corresponding pristine and OCV electrodes.

86-PL	Pristine electrode	OCV	3.8V	4.3V	4.6V	2.5V
At.% Carbon black (CB)	31.7	7.6	29.5	17.7	28.8	14.4
At.% PVDF	27.3	12.8	23.2	21.5	22.5	22.2
At.% Active material (AM)	3.8	3.0	3.8	4.4	6.0	6.0
At.% LiF/LixPFyOz	2.5	15.8	23.2	19.7	20.3	20.3
At.% Carbonaceous species	34.0	61.0	20.3	35.6	22.5	22.3

Table S8. Comparison of the contributions in atomic percentages of carbon black (CB), PVDF, active material (AM), $LiF/Li_xPF_yO_z$ species and carbonaceous species extracted from the global quantitative surface analyses performed from XPS spectra of electrodes made of the 17-PL sample and recovered at different states of charge and discharge during the 1st cycle. They are compared to the contributions obtained for the corresponding pristine and OCV electrodes.

17-PL	Pristine electrode	OCV	3.8V	4.3V	4.6V	2.5V
At.% Carbon black (CB)	32.0	11.2	13.1	7.8	12.3	16.5
At.% PVDF	26.8	15.6	19.3	13.3	13.9	15.3
At.% Active material (AM)	4.0	7.7	7.2	6.9	7.6	7.8
At.% $LiF/Li_xPF_yO_z$	2.3	22.6	27.5	32.7	37.6	34.6
At.% Carbonaceous species	34.2	44.5	32.8	39.9	28.5	25.6

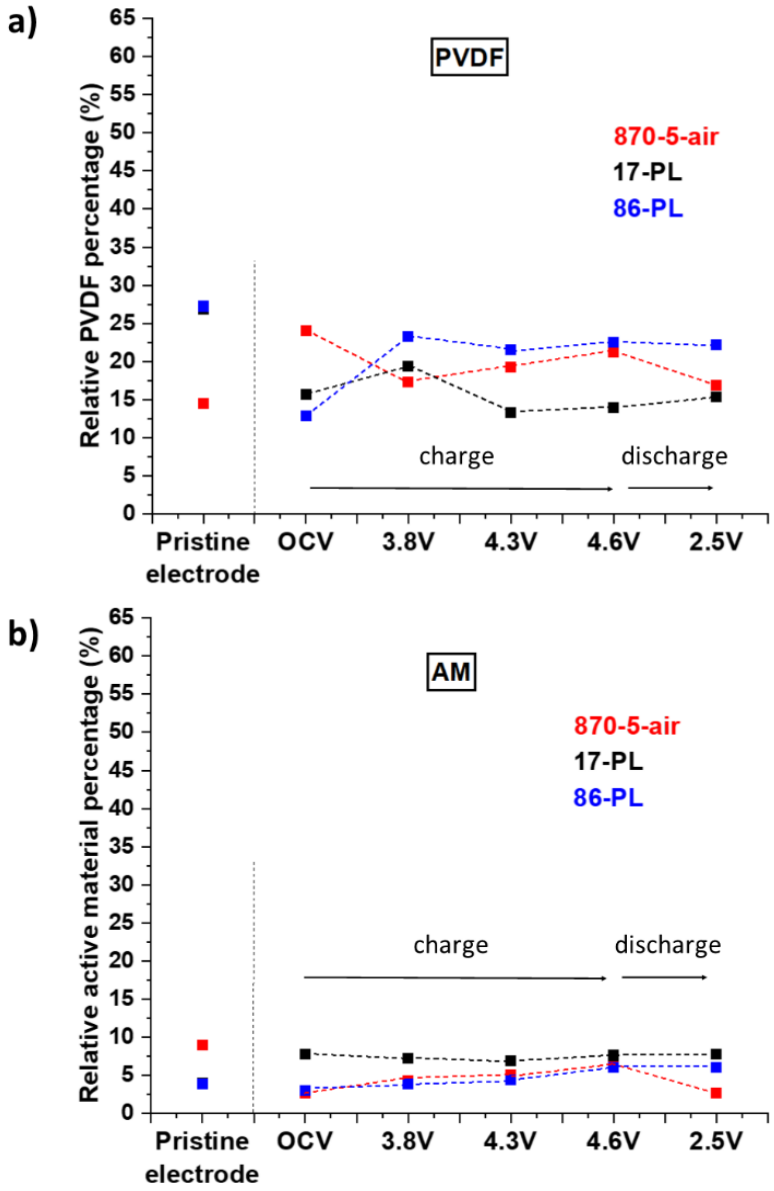

Figure S11. PVDF (a) and active material (b) proportions obtained from the XPS quantitative surface analyses performed on the 870-5-air (conventional particles), the 86-PL (86 nm thick platelets) and 17-PL (17 nm thick platelets) cycled electrodes.

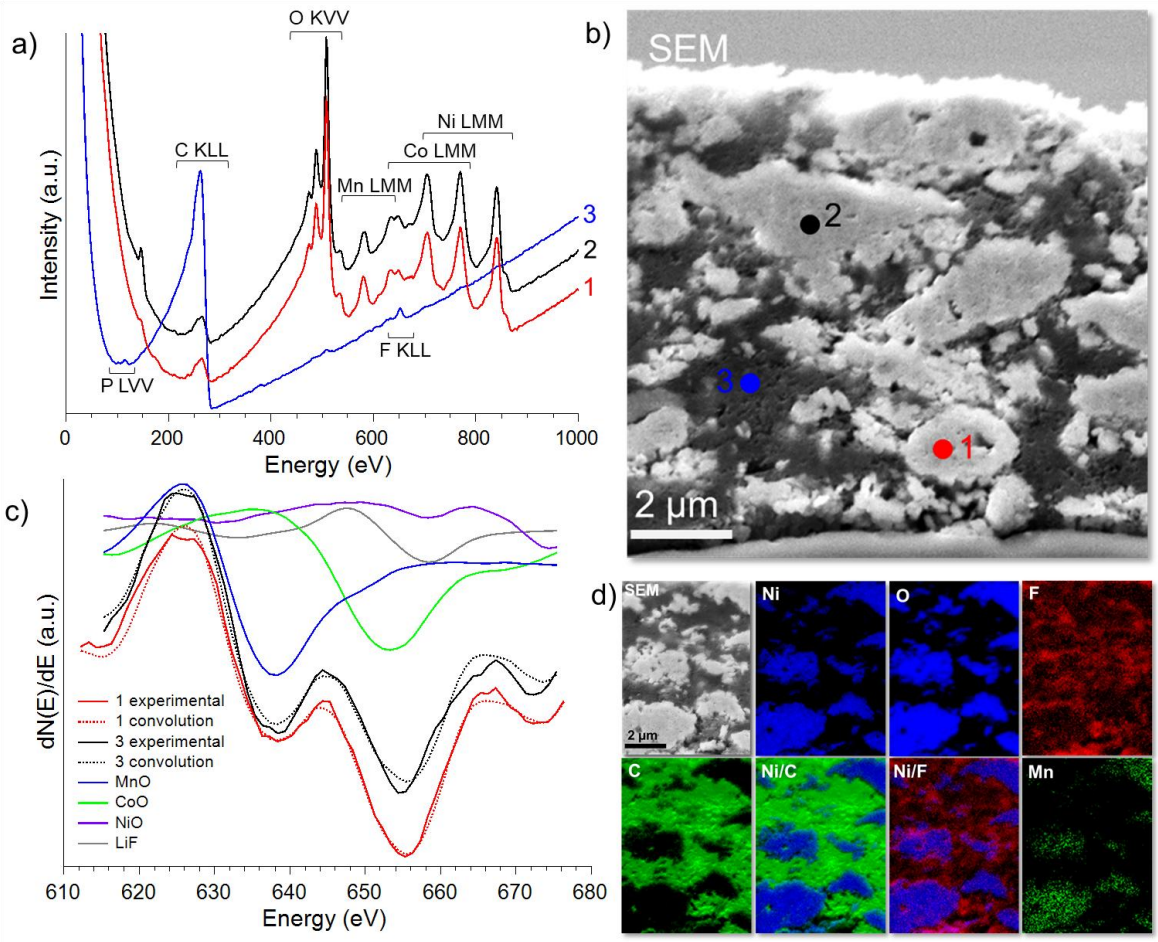

Figure S12. AES spectra (a) of three target dots on cross cut section of 86-PL (thick platelets) electrode (b). Derivative experimental spectra of dots 1 and 2 in the 600-670 eV energy region and their convoluted spectra obtained from the fitting with the MnO, CoO and LiF reference spectra (c) and SAM images of the cross cut section (d).

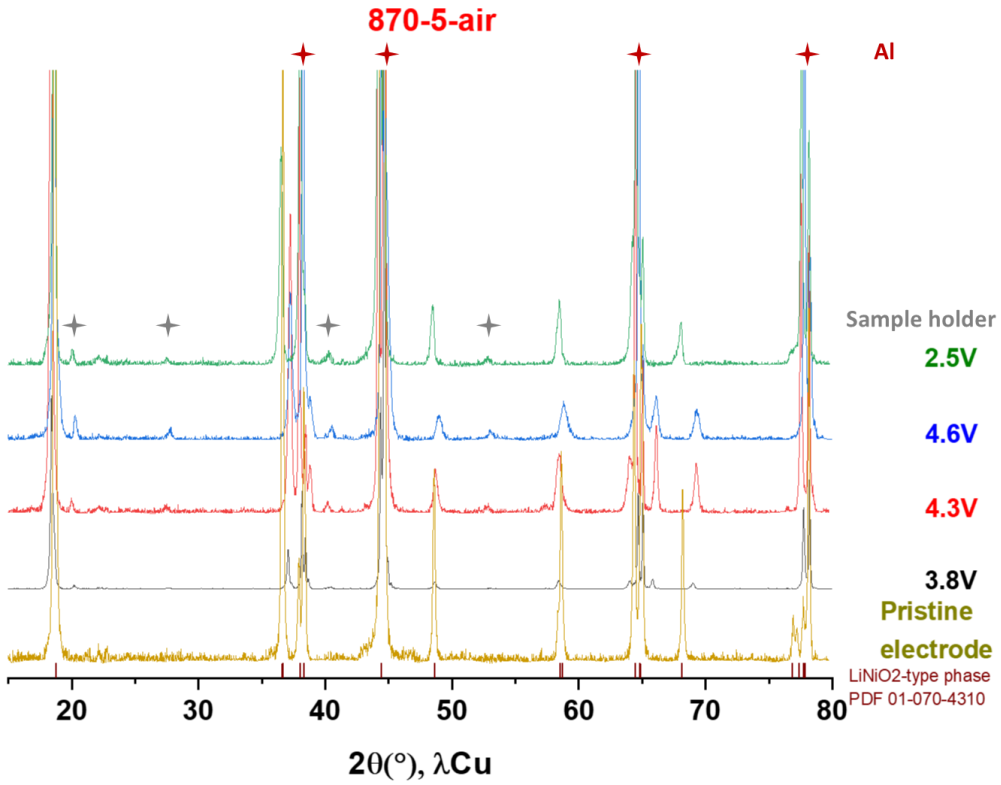

Figure S13. XRD patterns of the 870-5-air (with conventional particles) pristine and cycled electrodes recovered at 3.8 V, 4.3 V, 4.6 V and 2.5 V vs Li^+/Li. The peaks emphasized by red and grey stars are contributions coming from aluminum of the current collector and from the sample holder respectively.

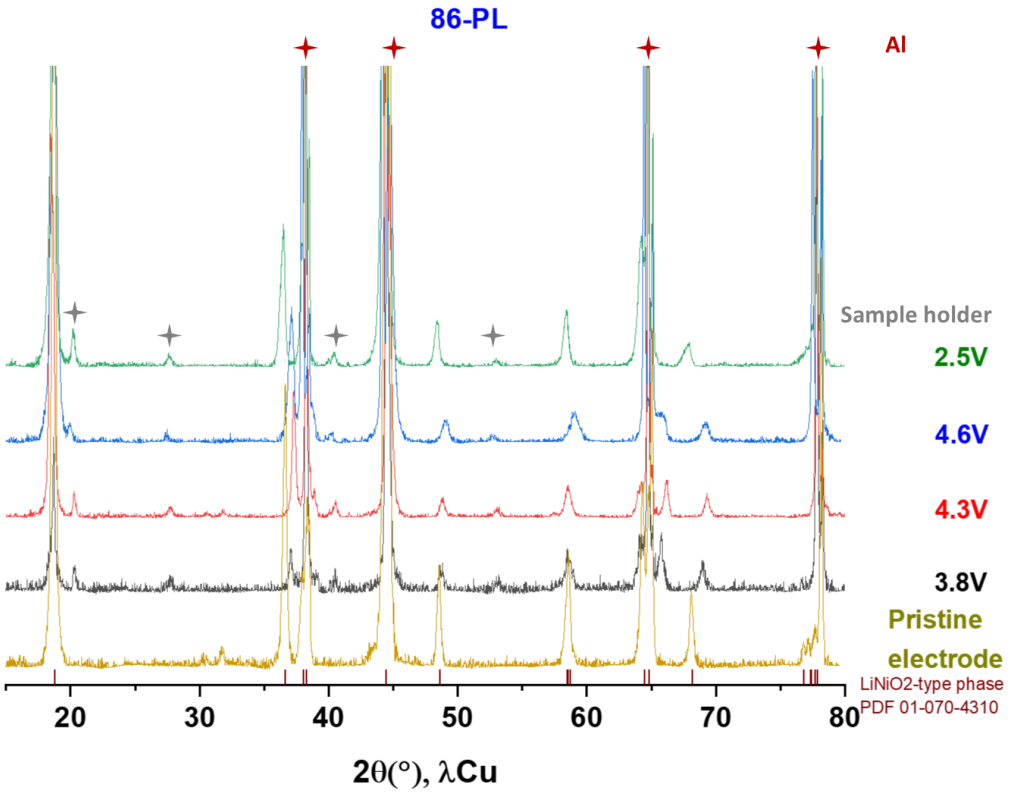

Figure S14. XRD patterns of the 86-PL (86 nm thick platelets) pristine and cycled electrodes recovered at 3.8 V, 4.3 V, 4.6 V and 2.5 V vs. Li^+/Li. The peaks emphasized by red and grey stars are contributions coming from aluminum of the current collector and from the sample holder respectively.

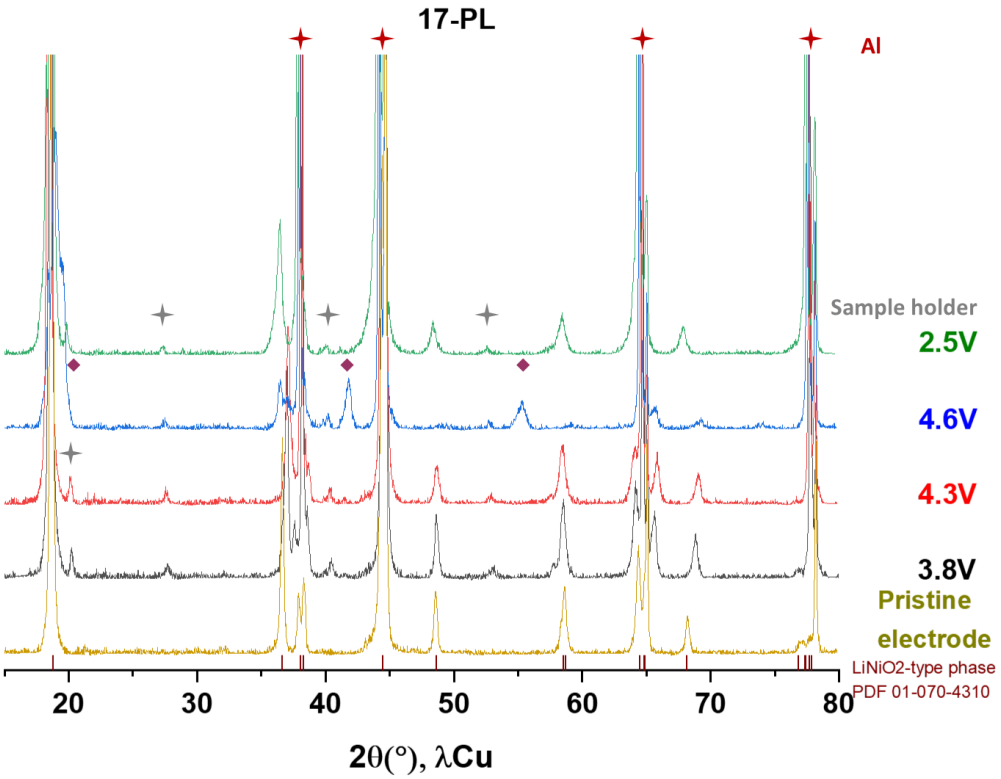

Figure S15. XRD patterns of the 17-PL (17 nm thick platelets) pristine and cycled electrodes recovered at 3.8 V, 4.3 V, 4.6 V and 2.5 V vs. Li^+/Li. The purple diamonds emphasize the characteristic peaks of the H4 phase (whose structure is described in the P-3m1 space group) identified at the end of charge. The peaks emphasized by red and grey stars are contributions coming from aluminum of the current collector and from the sample holder respectively.